Draft version July 22, 2019
Typeset using LaTeX **twocolumn** style in AASTeX62

Formation imprints in the kinematics of the Milky Way globular cluster system

Andrés E. Piatti[1,2]

[1] *Consejo Nacional de Investigaciones Científicas y Técnicas, Godoy Cruz 2290, C1425FQB, Buenos Aires, Argentina*
[2] *Observatorio Astronómico de Córdoba, Laprida 854, 5000, Córdoba, Argentina*

ABSTRACT

We report results on the kinematics of Milky Way (MW) globular clusters (GCs) based on updated space velocities for nearly the entire GC population. We found that a 3D space with the semi-major axis, the eccentricity and the inclination of the orbit with respect to the MW plane as its axes is helpful in order to dig into the formation of the GC system. We find that GCs formed *in-situ* show a clear correlation between their eccentricities and their orbital inclination in the sense that clusters with large eccentricities also have large inclinations. These GCs also show a correlation between their distance to the MW center and their eccentricity. Accreted GCs do not exhibit a relationship between eccentricity and inclination, but span a wide variety of inclinations at eccentricities larger than ~ 0.5. Finally, we computed the velocity anisotropy β of the GC system and found for GCs formed *in-situ* that β decreases from ≈ 0.8 down to 0.3 from the outermost regions towards the MW center, but remains fairly constant (0.7-0.9) for accreted ones. These findings can be explained if GCs formed from gas that collapsed radially in the outskirts, with preference for relative high infall angles. As the material reached the rotating forming disk, it became more circular and moved with lower inclination relative to the disk. A half of the GC population was accreted and deposited **in orbits covering the entire range of energies from the outer halo to the bulge.**

Keywords: globular clusters: general – Galaxy: formation – Galaxy: structure

1. INTRODUCTION

The study of the orbital motion of Milky Way (MW) globular clusters (GCs) has gained a renewed enthusiasm since the second data release (DR2) of the *Gaia* mission (Gaia Collaboration et al. 2016, 2018a) became publicly available (see, e.g. Li et al. 2018; Simpson 2019; Watkins et al. 2018). Previous studies of MW GC motions have shed some light on our knowledge about their formation and assembly history. For instance, Dinescu et al. (1999) obtained orbits for 38 GCs and found that some of them have large eccentricities and apogalactic distances larger than 10 kpc. They also found that internal two-body relaxation is more important than the destruction processes due to disk and bulge shocking. More recently, Pérez-Villegas et al. (2018) analyzed 9 bulge GCs and concluded that they move on rather eccentric prograde or retrograde orbits that are strongly influenced by the Galactic bar. A chaotization of the cluster orbits due to the MW bar was also found by Chemel et al. (2018) from the analysis of the motions of 115 GCs in a non-axisymmetric MW potential with a bar.

As far as we are aware, the most complete compilation of *Gaia* DR2 proper motions and ground-based line-of-sight velocities to date is that of Baumgardt et al. (2019)[1], who derived from them the space velocities of 156 GCs, and velocity dispersion profiles of 141 GCs. Their data set includes all GCs analyzed by Gaia Collaboration et al. (2018b) and Vasiliev (2019), respectively. Baumgardt et al. (2019) derived the total mass lost by GCs since their formation by computing their orbital motions backwards in time, accounting for mass-loss and dynamical friction. They found that the dynamical evolution plays an important role in the GC's mass loss process, in agreement with Dinescu et al. (1999). The derived Galactic positions (X, Y, Z), space velocities (U, V, W) and perigalactic (R_{peri}) and apogalactic (R_{apo}) distances can now be exploited to go forward in

Corresponding author: Andrés E. Piatti
e-mail: andres.piatti@unc.edu.ar

[1] Available at: https://people.smp.uq.edu.au/HolgerBaumgardt/globular/

our understanding of the dynamical behavior of the ancient Galactic GC system, and hence to draw some clues on the formation of the MW.

Precisely, in this work we comprehensively analyze the positions and velocities obtained by Baumgardt et al. (2019), and discuss the relationship between different orbital properties, in order to unveil possible scenarios of the events that took place during the formation of the MW. In Section 2 we derive the aforementioned kinematic properties, whereas Section 3 deals with the analysis of some relevant relationships and the comparison with recent results on different mechanisms of the GC formation. Finally, we summarize the main conclusions of this work in Section 4.

2. ORBITAL PROPERTIES

Several kinematic properties can be derived from the orbital parameters obtained by Baumgardt et al. (2019), namely: from the average values of R_{peri} and R_{apo} we define the mean semi-major axis of the GCs' orbits as:

$$a = \frac{R_{peri} + R_{apo}}{2}. \quad (1)$$

The semi-major axis has the advantage to be less time-dependant than the GC's Galactocentric distance (R_{GC}), and is more representative of the distance of a GC's birthplace to the Galactic center or the average distance where a GC was deposited after accretion of its host dwarf galaxy onto the MW. We also computed the orbital eccentricity (ϵ) as:

$$\epsilon = \frac{R_{apo} - R_{peri}}{R_{apo} + R_{peri}}; \quad (2)$$

the components of the angular momentum:

$$L_X = Y \times W - Z \times V, \quad (3)$$

$$L_Y = Z \times U - X \times W, \quad (4)$$

$$L_Z = X \times V - Y \times U; \quad (5)$$

and the inclination of the orbit:

$$i = acos\left(\frac{L_Z}{\sqrt{L_X^2 + L_Y^2 + L_Z^2}}\right). \quad (6)$$

Note that i values range from 0° for fully prograde in-plane orbits to 90° for polar orbits to 180° for in-plane retrograde orbits.

We also transformed the U, V and W space velocity components to the spherical ones V_r, V_θ and V_ϕ.

For each orbital property $f(x_1, x_2, ..., x_n)$, we derived its respective uncertainty through Monte Carlo simulations. We run one thousand computations of $f(x_1, x_2, ..., x_n)$ for each GC, each time using random values for all the involved independent variables x_i ($i = 1, ..., n$). These random values were choosing among all possible ones in the interval $[< x_i > -\sigma(x_i), < x_i > +\sigma(x_i)]$, where $< x_i >$ and $\sigma(x_i)$ are the mean values and errors of the involved cluster properties (variables) derived by Baumgardt et al. (2019). Then, we built a histogram from all the resulting $f(x_1, x_2, ..., x_n)$ values and considered as the uncertainty of $f(x_1, x_2, ..., x_n)$ 1/2 of the f range where more than 16% and less than 84% of the points are distributed.

Finally, we calculated the velocity anisotropy β. In doing this, we have first split the GC sample into three groups: $a \leq 3$ kpc (bulge); 3 kpc $< a \leq 20$ kpc (disk) and $a > 20$ kpc (outer halo). Then, we computed the velocity dispersions σV_r, σV_θ and σV_ϕ in V_r, V_θ and V_ϕ, respectively, using a maximum likelihood approach by optimising the probability $\mathcal{L}$ that the sample of selected GCs with velocities V_i and errors e_i are drawn from a population with mean $< V >$ and dispersion σ (e.g., Pryor & Meylan 1993; Walker et al. 2006), as follows:

$$\mathcal{L} = \prod_{i=1}^{N} \left(2\pi\,(e_i^2 + \sigma^2)\right)^{-\frac{1}{2}} \exp\left(-\frac{(V_i - < V >)^2}{2(e_i^2 + \sigma^2)}\right), \quad (7)$$

where the errors on the mean and dispersion were computed from the respective covariance matrices. Finally, we computed β as follows:

$$\beta = 1 - \frac{(\sigma V_\theta)^2 + (\sigma V_\phi)^2}{2(\sigma V_r)^2}, \quad (8)$$

We tried different relationships between the derived independent parameters, and found that using i versus ϵ versus $\log(a)$ results in the best enlightenment of the overall kinematic state of the GC system. Fig. 1 depicts this relationship for the GC sample. As can be seen, GCs with prograde orbits do not span the whole ranges of i and ϵ values randomly, but follow a general trend, in such a way that i increases with ϵ. There are a handful of GCs with prograde orbits with $\epsilon \gtrsim 0.5$ and $i \lesssim 25°$ that depart from this general relation, as well as some few GCs with $\epsilon \lesssim 0.3$ and $i \gtrsim 50°$. Regardless of these cases, the unveiled correlation shows that at a fixed eccentricity, the i range can vary (full range) between $\Delta(i) \sim 20°$ ($\epsilon \sim 0.2$) and $\Delta(i) \sim 80°$ ($\epsilon \sim 0.9$).

We interpret this behavior as if the present-day inclinations – along with the eccentricities and the semi-major axes – of the GC population have somehow kept imprints of their formation epoch. In general, they have orbits with large e and i values. For GCs with prograde orbits and 3 kpc $< a \leq 20$ kpc, we derived a Spearman

rank-order coefficient of 0.62 between their inclinations and their eccentricities, for those with $\epsilon < 0.5$ and $i < 50°$, 0.44, and for the whole prograde GC sample, we obtained 0.39. As for retrograde GCs, they have orbits with $\epsilon \gtrsim 0.5$ and with larger i values as their semi-major axes increase.

These features reveal that, independently of the direction of rotation (prograde or retrograde), GCs with more circular orbits tend to be more numerous in the inner parts than those in the outer parts of the Milky Way. In order to confirm such an orbital motion pattern, we plot in Fig. 2 the $(V_\phi^2 + V_\theta^2)/V^2$ ratio as a function of the semi-major axis. It shows that GCs with $\log(a$ /kpc$) \lesssim 0.8$ kpc are more numerous for $(V_\phi^2+V_\theta^2)/V^2 \gtrsim 0.8$. Note that this behavior is observed in GCs rotating in prograde and retrograde orbits.

The transition from nearly radial orbits of the outermost GCs to more or less disk-like rotating GCs in the MW main body (3 kpc $< a \leq$ 20 kpc) to the orbital anisotropy of the MW bulge GCs is also supported by the variation of the velocity anisotropy in terms of the distance from the Galactic center. We used the computed σV_r, σV_θ and σV_ϕ values as described above and then evaluated eq. (8). The resulting β values for the three distance ranges (bulge, disk, outer halo) turned out to be 0.29, 0.51 and 0.79 for prograde orbits of GCs formed *in-situ* (see also Section 3 for a discussion of GCs formed *in-situ*) and 0.72, 0.67 and 0.90 for retrograde ones, respectively, with typical $\sigma(\beta) \approx 0.1$. This result shows that while prograde orbits of GCs formed *in-situ* lose the radial imprints from the outer halo towards the bulge, the retrograde (accreted GCs, see Section 3) ones keep it throughout the whole MW.

3. ANALYSIS AND DISCUSSION

Nearly 75 per cent of the GCs have prograde orbits and they have mean i values of (70±20)° and (30±20)°, for outer halo and disk GCs, respectively. On the other hand, most of the GCs with retrograde orbits – thought to come from an accretion origin – have been able to keep their relatively high inclinations and eccentricities, even though some of them have reached very deep into the central regions of the MW (see Figs. 1 and 2). Here we make only use of the notion of accreted GCs described by Forbes & Bridges (2010) based on that retrograde motions are the signature of objects that have been accreted in the opposite rotational sense to the main bulk of Milky Ways rotation. Note that accreted GCs can also have prograde orbits, which we considered in the following analysis. For this reason, Forbes & Bridges (2010) also investigated the age-metallicity relationship as a diagnostic tool to disentangle accreted and formed

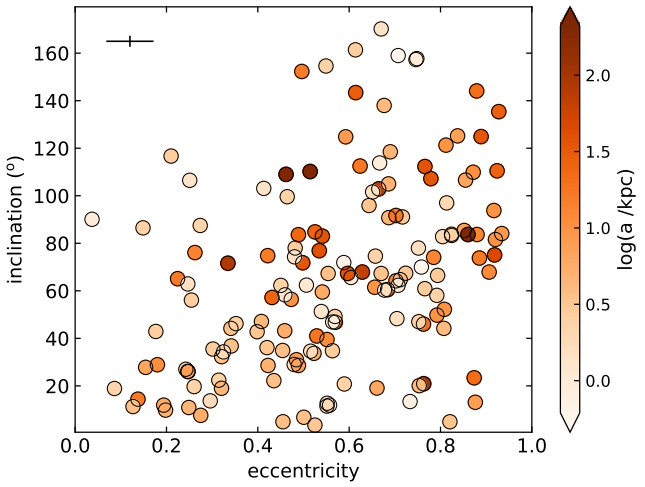

Figure 1. Relationship between the inclination (i) and the eccentricity (ϵ) for the GC sample. Symbols have been colored according to the color bar at the right margin. Typical error bars are also indicated.

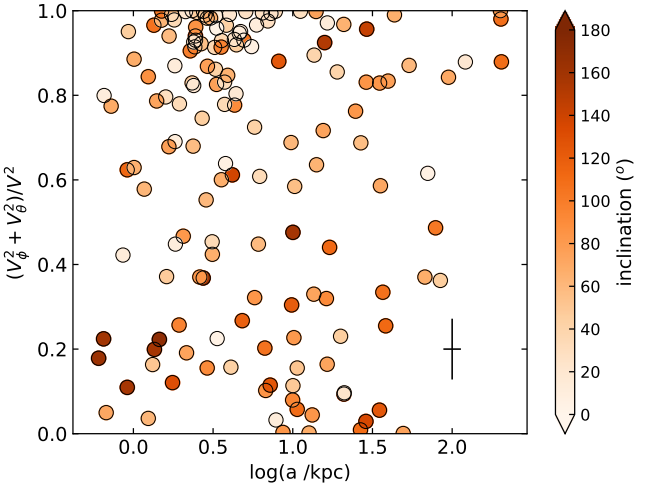

Figure 2. $(V_\phi^2 + V_\theta^2)/V^2$ ratio as a function of the semi-major axis for the GC sample. Typical error bars are also drawn.

in-situ GCs (see also Kruijssen et al. 2019). Since accreted GCs could also have prograde orbits, we assumed for them a similar number of objects as the GCs with retrograde orbits and with their same inclination distribution. Thus, we were able to subtract from the observed inclination distribution of prograde GCs that of retrograde GCs to obtain the distribution of prograde GCs formed *in-situ*.

We computed these inclination distributions of GCs in prograde and retrograde orbits for our three semi-major axis ranges. In order to build those distributions we considered each inclination as represented by a one-dimensional *Gaussian* of unity area centered at the re-

spective i value, with a FWHM/2.355 equals to the i error. Then, we used a grid of i bins with sizes of $\Delta(i)$ = 10° and added the fractions of the *Gaussians*' areas that fall into the bin boundaries. Thus, by taking into account the uncertainties of the i estimates, we were able to produce actual observed i distributions (not distributions coming from considering only mean individual i values) (see, e.g. Piatti 2014; Piatti et al. 2019). Fig. 3 shows the resulting distributions. As can be seen, there is a general different distribution of GCs in prograde orbits formed *in-situ* (bottom panel) with respect to those on retrograde GCs (middle panel). The latter show nearly similar inclination distributions in the three spatial ranges.

If we assumed that accreted GCs arrived uniformly from arbitrary directions, the distribution of their orbit poles would be uniform on a sphere. This means that the number of points at orbit poles $\sim 90°$ ($i \sim 0°$) should be smaller than that for orbit poles $\sim 0°$ ($i \sim 90°$). Precisely, Fig. 3 (middle panel) shows – at least for disk and outer halo GCs – that the larger the inclination, the larger the number of GCs, giving some support to the above assumption.

The outcome for GCs formed *in-situ* would imply that the initial collapse of gas out of which the GCs were formed was more or less isotropic – outer halo GCs have orbits spanning the whole range of inclinations –, and that, after the first disk passage, the motion of the gas became more circular and parallel to the Galactic plane – disk GCs have orbits with inclinations peaked at $\sim 30°$. In the bulge region, opposite currents of gas clashed, resulting in GCs spanning the whole range of eccentricities and inclinations (see also Figs. 1 and 2). Therefore, there could be a transition from mostly radial (outer MW) to more circular (inner MW) prograde orbits. Note that the formation of all these prograde GCs has happened in a space of time of $\lesssim 3$ Gyr (Kruijssen et al. 2019, and references therein). The accretion of GCs could have happened concurrently with the GC formation or a couple of Gyrs later (Helmi et al. 2018). Nevertheless, in either case, accreted GCs have not been fully subject of the angular momentum acquired by the early MW disk.

We have searched the literature seeking for any recent comprehensive model of the MW GC formation and found that most of the latest developments do not include kinematical GC signatures (see, e.g. Renaud et al. 2017; El-Badry et al. 2019). Binney & Wong (2017) developed a model of the hierarchical assembly of GCs and found that halo GCs show clearer rotation than their stellar counterpart; Fattahi et al. (2019) showed that halo metal-rich stars have highly eccentric orbits. The outcomes of Binney & Wong (2017) agree with our finding of more eccentric orbits for halo GCs. Nevertheless, the authors mentioned that their results are preliminary and that their analysis should be revisited.

Accretion of GCs has recently been more extensively discussed in the literature. Helmi et al. (2018) and Belokurov et al. (2018) claimed that only one major merger with a dwarf galaxy slightly more massive than the Small Magellanid Cloud was responsible for the formation of the MW think disk ~ 10 Gyr ago, while Pfeffer et al. (2018) and Kruijssen et al. (2019) introduced the accretion origin of GCs in a general cosmological context. Particularly, Kruijssen et al. (2019) found that the MW has experienced no major mergers since ~ 13 Gyr ago. Recently, Gallart et al. (2019) showed that there exist also an *in-situ* inner halo formed within the seed progenitor of the MW, just after the accreted inner halo population.

Helmi et al. (2018) associated to the merging dwarf galaxy Gaia-Enceladus 13 GCs (NGC 288, 362, 1851, 1904, 2298, 4833, 5139, 5286, 6205, 6341, 6779, 7089, 7099) with $L_z < 250$ kpc km/s, no mention whether their orbits are prograde or retrograde, but simply that they show a consistent age-metallicity relationship. However, the top-left panel of Fig. 4 highlights the positions of these GCs in the i versus ϵ plane, revealing that they have relatively large eccentricities and rotate in either prograde or retrograde orbits. In the case of Kruijssen et al. (2019), the authors identified three less massive dwarf progenitors each with a number of GCs associated to them, namely: Sagittarius (NGC 5634, 6715), Canis Major (NGC 1851, 1904, 2808, 4590, 5286, 6205, 6341, 6779, 7078, IC 4499) and Kraken (NGC 362, 1261, 3201, 5139, 5272, 5897, 5904, 5946, 6121, 6284, 6544, 6584, 6752, 6864, 6934, 6981, 7006, 7089). These GCs also have in general large eccentricities and are moving in either prograde or retrograde orbits (see top-right panel of Fig. 4). Gaia-Sausage is the same Gaia-Enceladus elongated structure in velocity space mentioned above, created by a massive dwarf galaxy ($\sim 5\times10^{10}$ $M_\odot$) on a strongly radial orbit that merged with the MW at a redshift $z \lesssim 3$ (Belokurov et al. 2018). Myeong et al. (2018) listed NGC 362, 1261, 1851, 1904, 2298, 2808, 5286, 6779, 6864 and 7089 as probable candidate GCs associated to Gaia-Sausage, showing a partial overlap with those listed by Helmi et al. (2018). We depicted them in the bottom-left panel of Fig. 4, showing that they also split into prograde and retrograde highly eccentric orbits. All candidate GCs with a dwarf origin have semi-major axes from ~ 5 up to 25 kpc and V_ϕ velocity components relatively small (see bottom-right panel of Fig. 4).

At this point, some unavoidable issues arise: firstly, there is an overlap of GCs associated to different host dwarf galaxies accreted onto the MW. Indeed, by comparing the list of GCs associated to Gaia-Sausage, Gaia-Enceladus, Sagittarius, Canis Major and Kraken, it is easy to identify those GCs included in two or three different lists. Myeong et al. (2018) used 6D information to search structures in action space of 91 GCs and a characteristic energy which separates the *in-situ* objects in Gaia-Sausage. Similarly, Helmi et al. (2018) constrained the azimuthal angular momentum L_z to be smaller than 250 kpc km/s, in addition to distances between 5 and 15 kpc from the Sun, and 40° away from the Galactic center to select GCs associated to Gaia-Enceladus. Finally, Kruijssen et al. (2019) based the selection of GCs associated to Sagittarius, Canis Major and Kraken on the reconstruction of the MW's merger tree from its GC age-metallicity distribution, and on the estimation of the number of mergers as a function of mass ratio and redshift. As can be inferred from the mentioned works, the partial agreement found between the outcomes of different selection procedures points to the need of further refinement.

Secondly, every group of associated GCs does not contain only GCs in retrograde orbital motions or in prograde ones, with the exception of Sagittarius. Gaia-Sausage and Canis Major have the same number of GCs with prograde/retrograde orbits, Gaia- Enceladus have a prograde/retrograde orbits ratio of 8:5, while Kraken 5:13. This means that either the selection of GCs associated to accreted dwarf galaxies based only on their angular momentum, or on their energies or on age-metallicity relationships is not enough as selection criteria. These astrophysical properties in addition to other properties would seem to be needed. Note, particularly, that two methods of selecting GCs associated to Gaia-Enceladus (= Gaia-Sausage) have obtained two different GC samples, with some overlap (Helmi et al. 2018; Myeong et al. 2018). If we assumed that any applied methods to find out GCs associated to accreted dwarf galaxies were robust, we should admit that GCs associated to the same accreted dwarf could have been deposited in retrograde/prograde orbits randomly.

Thirdly, according to Kruijssen et al. (2019) the ratio of accreted to *in-situ* GCs is $\sim 2/3$, i.e., nearly 40 per cent of the GC population was formed in dwarf galaxies. Here we assumed that the total number of accreted GCs is twice as big as that of GCs with retrograde orbits – we assigned the same probability to accreted GCs with prograde/retrograde orbits –, so that the accreted to *in-situ* GCs ratio turns out to be ~ 1. This ratio is ~ 1.5 times that of Kruijssen et al. (2019). Note that the present analysis does not favor GCs mainly being formed *in-situ*, nor accreted ones being observed only in the outer halo. It still remains an open issue whether the accreted GC population has been shaped by minor mergers (ratio 1:100 Kruijssen et al. 2019) or by one major merger event (ratio 1:4 Belokurov et al. 2018; Helmi et al. 2018).

Recently, several works have pointed out fairly large velocity anisotropy values (β) for the outer halo, and hence have characterized the motion of the halo stellar component like a more radial than a tangential subsystem. Bird et al. (2019) obtained $\beta \approx 0.9$ over the Galactocentric distance (R_{GC}) range 5 - 25 kpc for stars more metal-rich than [Fe/H] = -1.8 dex, and 0.6 for those more metal-poor (see also, Cunningham et al. (2018) ($\beta = 0.6$)). From $R_{GC} = 25$ kpc up to 100 kpc, Bird et al. (2019) found that β steadily decreases until ~ 0.3, independently of the metal content. Belokurov et al. (2018) agree with a high β value (0.9) for stars more metal-rich than [Fe/H] = -1.7 dex distributed within 10 kpc from the Sun. However, they derived a smaller one ($0.2< \beta <0.4$) for more metal-poor stars. Summing up, there seems to be a general agreement about the value of β as a function of the Galactocentric distance and its dependence on metallicity.

As for GCs, Binney & Wong (2017) found from a modeled GC system $\beta \sim 0.68$ at $R_{GC} = 12$ kpc with a steady decrease down to 0.53 at R_{GC} =30 kpc. Watkins et al. (2018) used 34 halo ones with distances to the MW center between 2.0 and 21.2 kpc and derived $\beta = 0.5$. Vasiliev (2018) derived a nearly constant $\beta \sim 0.6$ for $R_{GC} > 25$ kpc, and a decrease in the inwards direction down to $\beta \sim 0.4$ at $R_{GC} = 5$ kpc, and 0.0 at the MW center. The constant trend outwards 25 kpc does not match the decrease found by Bird et al. (2019), while for $R_{GC} < 25$ kpc, his value resembles those obtained from field stars more metal-poor than [Fe/H] < -1.7 dex (Bird et al. 2019; Cunningham et al. 2018; Watkins et al. 2018). Despite the small difference between the present GCs sample and that used by Vasiliev (2018), and the fact that we distinguished between prograde and retrograde orbits, our β values for GCs with prograde orbits are in fairly good agreement with his.

Finally, we analyzed the kinematics of the GC population in light of the MW rotation curve recently derived by Crosta et al. (2018, see also figure 16 in Bland-Hawthorn & Gerhard, 2016) (see Fig. 5). In the figure, we considered only GCs in prograde orbits. As can be seen, bulge GCs ($\log(a) < 0.2$) do have velocity components in the direction of the disk rotation smaller that those predicted for the MW bulge (red line). Here we speculate with the possibility that GCs and the MW

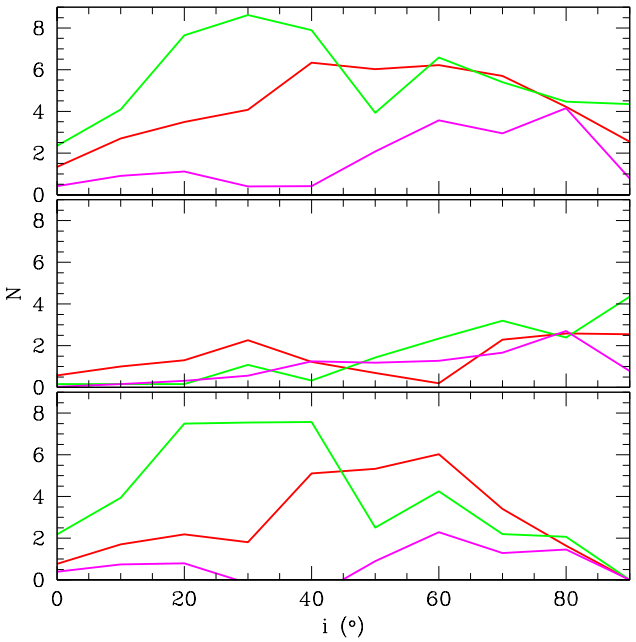

Figure 3. Distribution of observed prograde (top panel) and mirrowed (180°-i) retrograde (middle panel) GCs and prograde GCs formed *in-situ* (bottom panel) with semi-major axes (a) in the ranges: $a \leq 3$ kpc (red line), 3 kpc $< a \leq 20$ kpc (lime line) and $a > 20$ kpc (magenta line), respectively.

bulge do not share similar kinematics in the direction of the disk rotation or that there still are bulge GCs not found (see, e.g. Ryu & Lee 2018; Camargo 2018). For GCs spread throughout the MW's disk, their velocity components in the direction of the disk rotation span the whole range below the total MW rotation curve. As we mentioned above, they have been formed from gas that fell increasingly circularized into the growing disk, hence the dispersion in their circular velocities. There is also a group of GCs that have V_ϕ values higher than $\sim$ 250 km/s. They have eccentric orbits and fall outside the mean correlation of Fig. 1, and could have an accretion origin.

4. CONCLUSIONS

In this work we take advantage of the catalogue of space velocities for nearly all confirmed MW GC population built recently by Baumgardt et al. (2019), aiming at studying the global kinematic properties of them as one of the ancient Galactic subsystems. Previous attempts have been constrained by the smaller number of GCs with accurate proper motions and line-of-sight velocities, among others.

We show that the relationship between the eccentricity and the inclination of the GC orbits sheds light on the possible sequence of events that occurred when the Galactic GC system formed. Although the calculated inclinations refer to the present-day values, it seems that, for prograte orbits and 3 kpc $< a \leq 20$ kpc, they vary at most $\sim 10°$ around the mean value at a fixed eccentricity. This behavior makes the inclination of the GC orbit a useful time-independent orbital parameter. Indeed, the resulting linear relationship between the eccentricity and the inclination of prograde orbits suggests that the larger the eccentricity the higher the inclination. This trend resulted to be also a function of the semi-major axis (or averaged Galactocentric distance), so that the outermost GCs have the orbits with the highest inclinations respect to the Galactic plane and large eccentricity. For GCs with retrograde orbits, which represent 1/3 of those with prograde orbits, there is mostly dispersion over the whole inclination range for eccentricities larger than $\sim$ 0.5.

The eccentricity versus inclination relationship for GCs rotating in prograde orbits reveals that the initial collapse of the gas that gave birth to the MW GCs was geometrically radial with preference for relative high angles respect to the Galactic plane. As the gas reached the growing rotating disk, it became more circular and parallel to it. Hence, GCs that have been formed in the outskirts of the MW have very eccentric and highly inclined orbits, whereas those belonging to the disk show direction of movements more similar to that of the disk. As for GCs with retrograde highly eccentric orbits, they have likely an origin of accretion. Nevertheless, we also identified GCs with prograde highly eccentric orbits that could have been accreted.

The more eccentric orbits of the outermost GCs in comparison with those of the disk GCs, is also supported by the resulting velocity anisotropy (β). Particularly, we computed β for three semi-major axis (a) ranges, namely: the innermost GCs ($a \leq 3$ kpc), GCs spanning the extension of the Galactic disk (3kpc$< a \leq$20 kpc) and outer halo GCs ($a>$ 20 kpc). We found that β decreases from 0.79 down to 0.29 towards the Galactic center for prograde GCs. In the case of GCs on retrograde orbits, β remains nearly constant (0.75).

I thank Holger Baumgardt for providing me with his globular cluster database and contributed to improve the paper and the referee for the thorough reading of the manuscript and timely suggestions to improve it.

REFERENCES

Baumgardt, H., Hilker, M., Sollima, A., & Bellini, A. 2019, MNRAS, 482, 5138, doi: 10.1093/mnras/sty2997

Belokurov, V., Erkal, D., Evans, N. W., Koposov, S. E., & Deason, A. J. 2018, MNRAS, 478, 611, doi: 10.1093/mnras/sty982

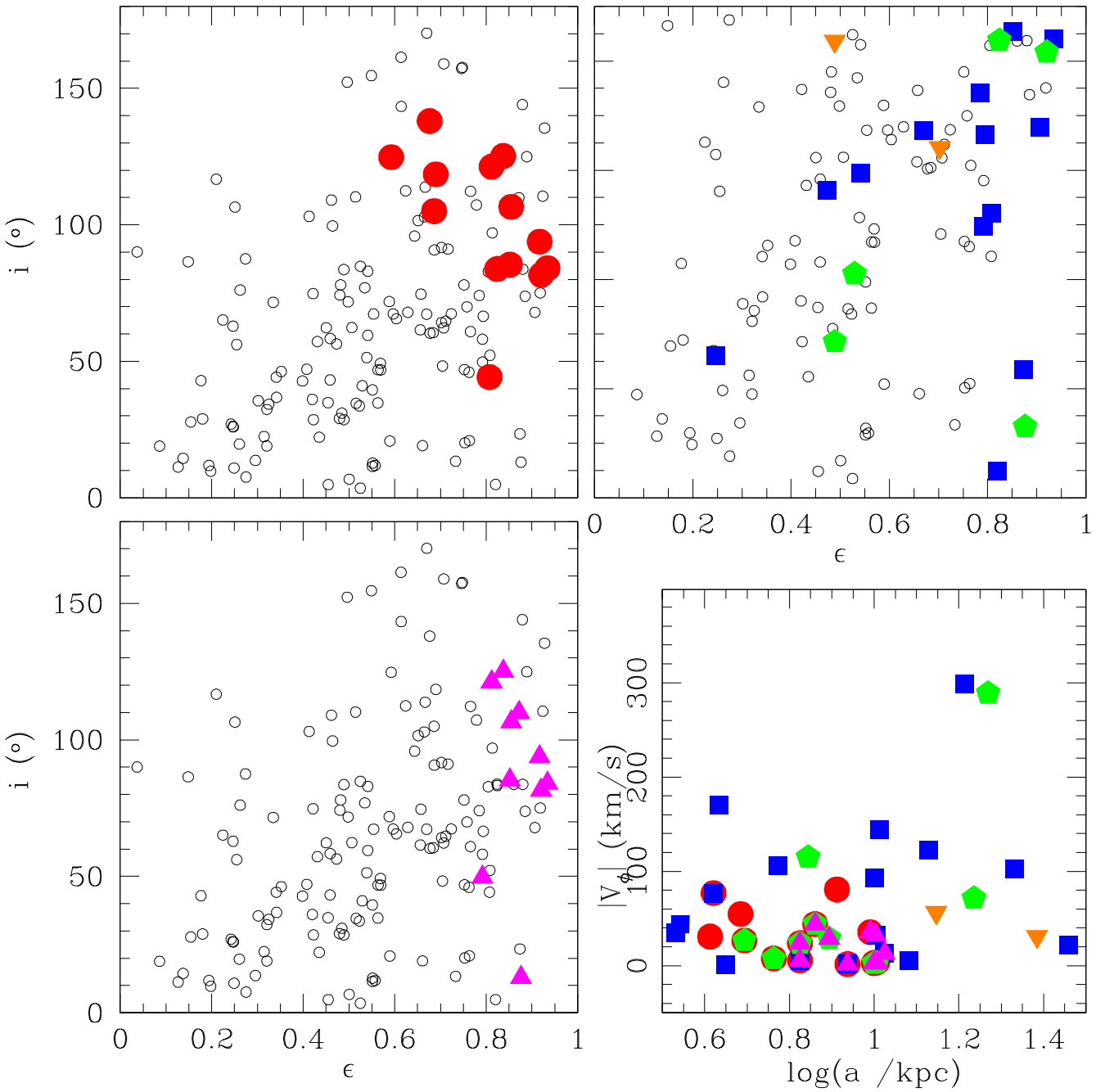

Figure 4. Relationship between the inclination (i) and the eccentricity (ϵ) for the GC sample. GCs associated to Gaia-Enceladus (top-left panel, red symbols), Kraken, Canis Major and Sagittarius (top-right panel. blue, lime and orange symbols, respectively) and Gaia-Sausage (bottom-left panel, magenta symbols) are indicated. The bottom-right panel shows only colored symbols in the three other panels (see text in Sect. 3).

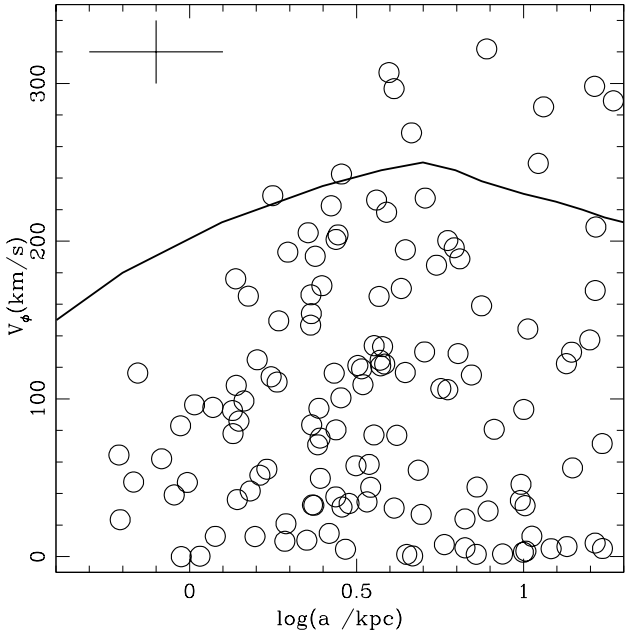

Figure 5. Total circular velocity curve of the MW derived by Crosta et al. (2018). Open circles represent GCs in prograde orbits. Typical error bars are also indicated.

Binney, J., & Wong, L. K. 2017, MNRAS, 467, 2446, doi: 10.1093/mnras/stx234

Bird, S. A., Xue, X.-X., Liu, C., et al. 2019, AJ, 157, 104, doi: 10.3847/1538-3881/aafd2e

Camargo, D. 2018, ApJL, 860, L27, doi: 10.3847/2041-8213/aacc68

Chemel, A. A., Glushkova, E. V., Dambis, A. K., et al. 2018, Astrophysical Bulletin, 73, 162, doi: 10.1134/S1990341318020049

Crosta, M., Giammaria, M., Lattanzi, M. G., & Poggio, E. 2018, arXiv e-prints, arXiv:1810.04445. https://arxiv.org/abs/1810.04445

Cunningham, E. C., Deason, A. J., Sanderson, R. E., et al. 2018, arXiv e-prints. https://arxiv.org/abs/1810.12201

Dinescu, D. I., Girard, T. M., & van Altena, W. F. 1999, AJ, 117, 1792, doi: 10.1086/300807

El-Badry, K., Quataert, E., Weisz, D. R., Choksi, N., & Boylan-Kolchin, M. 2019, MNRAS, 482, 4528, doi: 10.1093/mnras/sty3007

Fattahi, A., Belokurov, V., Deason, A. J., et al. 2019, MNRAS, 484, 4471, doi: 10.1093/mnras/stz159

Forbes, D. A., & Bridges, T. 2010, MNRAS, 404, 1203, doi: 10.1111/j.1365-2966.2010.16373.x

Gaia Collaboration, Prusti, T., de Bruijne, J. H. J., et al. 2016, A&A, 595, A1, doi: 10.1051/0004-6361/201629272

Gaia Collaboration, Brown, A. G. A., Vallenari, A., et al. 2018a, A&A, 616, A1, doi: 10.1051/0004-6361/201833051

Gaia Collaboration, Helmi, A., van Leeuwen, F., et al. 2018b, A&A, 616, A12, doi: 10.1051/0004-6361/201832698

Gallart, C., Bernard, E. J., Brook, C. B., et al. 2019, arXiv e-prints. https://arxiv.org/abs/1901.02900

Helmi, A., Babusiaux, C., Koppelman, H. H., et al. 2018, Nature, 563, 85, doi: 10.1038/s41586-018-0625-x

Kruijssen, J. M. D., Pfeffer, J. L., Reina-Campos, M., Crain, R. A., & Bastian, N. 2019, MNRAS, 486, 3180, doi: 10.1093/mnras/sty1609

Li, G.-W., Yanny, B., & Wu, Y. 2018, ApJ, 869, 122, doi: 10.3847/1538-4357/aaed29

Myeong, G. C., Evans, N. W., Belokurov, V., Sanders, J. L., & Koposov, S. E. 2018, ApJL, 863, L28, doi: 10.3847/2041-8213/aad7f7

Pérez-Villegas, A., Rossi, L., Ortolani, S., et al. 2018, PASA, 35, e021, doi: 10.1017/pasa.2018.16

Pfeffer, J., Kruijssen, J. M. D., Crain, R. A., & Bastian, N. 2018, MNRAS, 475, 4309, doi: 10.1093/mnras/stx3124

Piatti, A. E. 2014, MNRAS, 437, 1646, doi: 10.1093/mnras/stt1998

Piatti, A. E., Salinas, R., & Grebel, E. K. 2019, MNRAS, 482, 980, doi: 10.1093/mnras/sty2761

Pryor, C., & Meylan, G. 1993, in Astronomical Society of the Pacific Conference Series, Vol. 50, Structure and Dynamics of Globular Clusters, ed. S. G. Djorgovski & G. Meylan, 357

Renaud, F., Agertz, O., & Gieles, M. 2017, MNRAS, 465, 3622, doi: 10.1093/mnras/stw2969

Ryu, J., & Lee, M. G. 2018, ApJL, 863, L38, doi: 10.3847/2041-8213/aad8b7

Simpson, J. D. 2019, arXiv e-prints. https://arxiv.org/abs/1902.00447

Vasiliev, E. 2018, MNRAS, 481, L100, doi: 10.1093/mnrasl/sly168

—. 2019, MNRAS, 484, 2832, doi: 10.1093/mnras/stz171

Walker, M. G., Mateo, M., Olszewski, E. W., et al. 2006, AJ, 131, 2114, doi: 10.1086/500193

Watkins, L. L., van der Marel, R. P., Sohn, S. T., & Evans, N. W. 2018, arXiv e-prints. https://arxiv.org/abs/1804.11348